

Mid-Infrared Imaging of the Protostellar Binary L1448N–IRS3(A,B)

David R. Ciardi, Jonathan P. Williams¹, Charles M. Telesco

*211 Space Sciences Building, Department of Astronomy, University of Florida, Gainesville,
FL 32611*

ciardi@astro.ufl.edu, jpw@ifh.hawaii.edu, telesco@astro.ufl.edu

R. Scott Fisher

Gemini Observatory, 670 North A’ohoku Place, Hilo, HI 96720-2700

sfisher@gemini.edu

Chris Packham, Robert Piña, James Radomski

*211 Space Sciences Building, Department of Astronomy, University of Florida, Gainesville,
FL 32611*

packham@astro.ufl.edu, rpina@astro.ufl.edu, jtr@astro.ufl.edu

ABSTRACT

Mid-infrared (10 – 25 μm) imaging of the protostellar binary system L1448N-IRS3(A,B) is presented. Only one source, IRS3(A), was detected at mid-infrared wavelengths – all of the mid-infrared emission from IRS3(A,B) emanates from IRS3(A). The mid-infrared luminosity of IRS3(A) is $L_{\text{midir}} = 1.3 \left(\frac{d}{300\text{pc}}\right)^2 L_{\odot}$, which yields a central source mass, depending on the mass infall rate, of $M_{\star} = 0.2 M_{\odot} \frac{10^{-6} M_{\odot} \text{yr}^{-1}}{\dot{M}}$. The envelope mass surrounding IRS3(A) is $\sim 0.15 M_{\odot}$, suggesting that the central source and the envelope are of comparable mass. The locations of IRS3(A) and IRS3(B) on an $M_{\text{env}} - L_{\text{bol}}$ diagram indicate that IRS3(A) and IRS3(B) appear to be class I and class 0 protostars, respectively.

Subject headings: infrared: ISM — infrared: stars — ISM: individual (L1448, L1448N-IRS3) stars: formation — stars: pre-main-sequence

¹Current Address: Institute for Astronomy, 2680 Woodlawn Drive Honolulu, HI 96822

1. Introduction

Protostars are young stellar objects that are still in the process of accreting the bulk of material, and with most of their luminosity being derived from the infall of matter. Class I young stellar objects (Lada & Wilking 1984; Lada 1987) have been viewed as protostellar candidates (Adams, Lada, Shu 1987), but sub-mm work showed that many class I objects have lower mass envelopes than expected, suggesting that these class I objects may have already depleted their surrounding envelopes (e.g., Barsony & Kenyon 1992).

Class 0 sources were identified by André, Ward-Thompson, & Barsony (1993) as sources that are more deeply embedded and associated with more powerful outflows than “standard” class I young stellar objects. Consequently, the class 0 sources have been proposed as the evolutionary precursors to the class I protostars (André, Ward-Thompson, & Barsony 1993; André & Montmerle 1994). Work by Bontemps et al. (1996) and Saraceno et al. (1996) suggested a direct evolutionary sequence from the class 0 stage to the class I stage, with the class 0 sources representing the youngest protostars. Observationally, the defining characteristics of the class 0 sources are 1) a submillimeter-to-bolometric luminosity ratio of $\gtrsim 0.5\%$, 2) invisibility at near-infrared wavelengths, 3) a spectral energy distribution (SED) described by a single-temperature (modified) blackbody with a bolometric temperature of $T < 70$ K, and 4) the presence of a molecular outflow (André, Ward-Thompson, & Barsony 2000; Chen et al. 1995, 1997).

However, recently Jayawardhana, Hartmann, & Calvet (2001) have argued that class 0 protostars are located preferentially in higher density regions and that class I young stellar objects are located preferentially in lower density regions and may be of comparable evolution. Thus, the class 0 and class I sources may not represent a true evolutionary sequence. To further complicate the distinction between class 0 and class I objects, some class I objects, which are viewed at high inclination, may appear “class 0-like” because of the high optical depth associated with viewing the disk around class I sources (nearly) edge-on (Masunaga & Inutsuka 2000).

To help address these issues, it would be instructive to study a set of young stellar objects believed to be coeval and located within the same environment, thus removing the possible ambiguity of differing initial conditions. The binary system L1448N-IRS3 may provide such a useful comparison.

L1448 is a globule located within the Perseus molecular cloud complex ($d \sim 300$ pc) containing an extremely young and highly collimated bipolar outflow (Bachiller et al. 1990). The exciting source (L1448-mm) of the bipolar outflow was identified by Curiel et al. (1990), and has been classified as a class 0 protostar. Located in the northwest portion of the bipolar

outflow is the infrared source L1448N-IRS3, which is powering its own molecular outflow (Guilloteau et al. 1992; Davis & Smith 1995).

L1448N-IRS3 consists of three sources which have been resolved at mm wavelengths (e.g., Looney, Mundy, & Welch 2000) and are known as L1448N-IRS3(A), L1448N-IRS3(B), and L1448N-IRS3(C). L1448N-IRS3(C), also known as L1448NW, is located $\sim 20''$ northwest of IRS3(A,B), and is not considered in this paper. IRS3(A) and IRS3(B) are separated by $\sim 7''$ (2100 AU) and are considered a coeval, protostellar binary system with a common envelope (Terebey & Padgett 1997; Barsony et al. 1998). It has been suggested that the strong bipolar outflow from L1448-mm may have induced the star formation associated with L1448N-IRS3 (Barsony et al. 1998).

Taken together, the IRS3(A,B) binary meets each of the observational requirements for a class 0 protostar: 1) $L_{submm}/L_{bol} \approx 3\%$ (Barsony et al. 1998); 2) neither of the sources has been detected at K to a limit of 18th magnitude (Terebey & Padgett 1997); 3) the mm SED is characterized by a temperature of 22.5 K (Barsony et al. 1998); and 4) there is a molecular outflow associated with the system (Guilloteau et al. 1992). Detailed modeling of IRS3(A,B) has been performed on the binary as a whole (e.g., Shirley et al. 2000), and consequently, the relative evolutionary status of the individual components of IRS3 remains undetermined.

There are differences between the two sources. At 2.7 mm, IRS3(B) is the stronger source ($F_A/F_B \approx 0.17$; Looney, Mundy, & Welch 2000), while at 2 and 6 cm, IRS3(A) dominates the emission ($F_A/F_B \approx 3$; Curiel et al. 1990). The derived envelope masses from the resolved (optically thin) mm data are $0.09 M_\odot$ and $0.52 M_\odot$, for IRS3(A) and IRS3(B), respectively. While both sources are apparently associated with outflows (Davis & Smith 1995; Barsony et al. 1998), only IRS3(B) displays signatures of mass infall, suggesting that IRS3(A) may have accumulated most of its envelope mass (Terebey & Padgett 1997). The two sources remain unresolved for all other observations (mm wavelengths 1.3 – 2.6 mm; Terebey, Chandler, & André (1993), and IRAS infrared wavelengths; Barsony et al. (1998)). The binary system has a combined bolometric luminosity of $L \approx 10.9 L_\odot$. Barsony et al. (1998) note that the IRAS infrared emission appears in excess of that expected from the single-temperature blackbody fit to the mm data, and they attribute the excess to shock-heated dust associated with the outflows.

Millimeter wavelengths are most sensitive to the cool outer envelopes surrounding protostars. Complementary to mm observations, mid-infrared observations probe the inner regions of accretion near, or at, the central protostar and are expected to have only a minor contribution from the outer envelope. Thus, observations at $10 - 25 \mu\text{m}$ provide a means of comparing the central protostar to the outer envelope. The IRAS observations do not

spatially resolve the components of IRS3 (Barsony et al. 1998). So while IRS3(A,B) is relatively bright at mid-infrared wavelengths ($F_{12\mu\text{m}} \approx 0.6$ Jy, $F_{25\mu\text{m}} \approx 6$ Jy), it is unclear how the mid-infrared emission is distributed among the two sources and the envelope.

In order to disentangle the mid-infrared emissions from IRS3(A), IRS3(B), and the envelope, and to clarify the evolutionary status of the sources, we present mid-infrared (10 – 25 μm) high-angular-resolution ($\sim 0.5''$) observations of the protostellar binary system. Only IRS3(A) was detected; upper limits for the mid-infrared emission of IRS3(B) are discussed. We calculate regional and bolometric luminosities, and estimate the central and envelope masses. We conclude with a brief discussion of the evolutionary status of the sources.

2. Observations and Data Reduction

Observations of IRS3 were made on 05 December 2000 UT using the University of Florida mid-infrared camera OSCIR on the Gemini-North 8 m telescope. OSCIR utilizes a 128×128 Si:As blocked impurity band detector, with a pixel scale of $0''.089$ per pixel and a field of view of $11''.4 \times 11''.4$ on the Gemini-North telescope. IRS3 was observed in four filter passbands (N, IHW18, Q3, & H25) using a standard chop-nod sequence with a $30''$ chop throw in declination. The weather was mostly clear with some high cirrus and typical seeing of $< 0''.5$. A summary of the filters, frametimes, total integration time per filter, and associated airmasses is given in Table 1.

To ensure accurate pointing, the telescope was first centered on the optical guide star located $\sim 5'$ from IRS3, and the telescope was offset to a position located directly between IRS3(A) and IRS3(B). The initial source acquisition was made with the H25 filter ($\lambda_c \sim 24 \mu\text{m}$). The flux calibration was obtained by observing β And just prior to the science observations and α Tau just after the science observations.

IRS3(A) was immediately apparent in the real-time OSCIR data acquisition quick-look display. To remove the possibility of pointing errors and ambiguity of the identity of the detected source, the offset pointing was confirmed and a three-position mosaic was made with the H25 filter, with $5''$ steps to the northwest. No detection of IRS3(B) or any other source was made. The data were reduced with custom-written IDL routines for the OSCIR data format. The images were smoothed with an $0''.4$ gaussian, and standard aperture photometry was performed on the final reduced co-added frames using an IDL version of PHOT, with an aperture diameter of $0''.75$. The H25 ($24 \mu\text{m}$) mosaic is presented in Figure 1.

3. Discussion

The primary result, as indicated by Figure 1, is that *all* of the mid-infrared flux observed from L1448N-IRS3 emanates from IRS3(A). All of the detected flux arises within a region of diameter $0''.75$; i.e., the mid-infrared emission comes from a region located *no farther* than ~ 100 AU, in projection, from the central source. Barsony et al. (1998) argued that the infrared emission (12 & 25 μm), in excess of the envelope contribution, may be the result of shock-heated dust resulting from interactions between the local dust and the outflows. No mid-infrared emission is observed toward IRS3(B), which powers its own outflow, or in the general environment, suggesting that the mid-infrared emission of IRS3 is associated entirely with the accretion emission of IRS3(A).

Figure 1 does show a hint of extended structure at 24 μm which is perpendicular to the direction of the H_2 outflow emission from IRS3 (Davis et al. 1994), perhaps suggestive of the accretion structure around IRS3(A). The other mid-infrared images were searched for evidence of this structure, and nothing conclusive was found. However, the integration time for the 24 μm image is 3 times longer than the integrations times in other filters. At present, it is unclear if the observed structure is real.

3.1. Mid-Infrared Spectral Energy Distribution

The photometry for IRS3(A) is presented in Table 2, and is in agreement with the IRAS HIRES flux densities reported in Barsony et al. (1998). While IRS3(B) was not detected, 3σ upper limits were calculated based upon the statistical uncertainties of photometry for IRS3(A). In addition to the OSCIR data presented here, the ISO database was searched, and a 14 μm ISOCAM image was extracted. ISO clearly detected IRS3, but did not resolve the two sources. Here we assume that the ISO 14 μm emission is contributed solely by IRS3(A), as is the case for our mid-infrared photometry. Using a $20''$ aperture, the 14 μm flux density is measured to be $F_{14\mu\text{m}} = 0.5 \pm 0.1$ Jy. The OSCIR and ISO mid-infrared SED of IRS3(A) is displayed in Figure 2.

To understand the temperatures associated with the mid-infrared emission, a single temperature blackbody was fitted to the dataset. A $T = 148 \pm 6$ K blackbody² characterizes

²Uncertainties for the blackbody fitting were estimated via a Monte Carlo simulation where the data points were randomly adjusted by their individual uncertainties, and the data were re-fitted. The simulation was performed 5000 times, and the final uncertainties were estimated from the standard deviations of the best fits.

the overall 10 – 25 μm colors, but is generally a poor fit to the dataset with a $\chi^2 \sim 11$. In the SED plot (Fig. 2), the $T \sim 148$ K blackbody curve is shown, and it clearly does not represent accurately the distribution of the mid-infrared fluxes.

If the blackbody fitting is restricted to the $\lambda > 18$ μm data, a single temperature $T = 82 \pm 9$ K blackbody fits the longer wavelength data very well ($\chi_\nu^2 \sim 0.3$), but significantly underestimates the 10 & 14 μm fluxes (see Fig. 2). We also considered a single-temperature modified blackbody function of the form $S_\nu = B_\nu(T_d)(1 - e^{-\tau_\nu})\Omega$, where $B_\nu(T_d)$ is the Planck function, τ_ν is the optical depth with a ν^β dependency, and Ω is the solid angle. However, we did not find a reasonable fit to the dataset. In order to parameterize the observations, multiple source temperatures are necessary.

A two temperature blackbody function of the form $S_\nu(T_1, T_2) = s \cdot [f \cdot B_\nu(T_1) + (1 - f) \cdot B_\nu(T_2)]$, where T_1 and T_2 are the blackbody temperatures, s is the scaling factor, and f is the fractional contribution of the primary blackbody component, was fitted to the mid-infrared data. In general, the scaling factor s is a multiplicative combination of the source solid angle and the radiative transfer function $(1 - e^{-\tau})$. The relative contributions f and $(1 - f)$ may represent source size and/or optical depth differences. As a final caveat, the broad N-band 10 μm filter and the ISO 14 μm filter span the silicate feature. Without narrow-band photometry or low-resolution spectroscopy, it is not possible to determine how the silicate feature contaminates the photometry. Since the silicate feature, if present, is likely to be in absorption for such young and highly embedded sources, the 10 and 14 μm fluxes may underestimate the overall mid-infrared continuum level.

The best fit parameters for the dual-blackbody model consist of two distinct temperatures of $T_1 = 71 \pm 8$ K and $T_2 = 240 \pm 59$ K with relative contributions of $f = 99.98\%$ and $(1 - f) = 0.02\%$, and a scale factor of $s = 9.4 \times 10^{-12}$. The resultant reduced chi-square is $\chi_\nu^2 = 0.2$. The summed curve and the individual components of the fit are shown in Fig. 2.

A two temperature blackbody model is obviously simplistic given that the temperature distribution is likely to be continuous with, for example, a radial powerlaw fall-off of the form $T(r) \propto r^{-0.4}$ (Kenyon, Calvet, & Hartmann 1993; Terebey, Chandler, & André 1993). However, it does characterize the emission and emphasizes the regions from where the mid-infrared emission arises. Dust temperatures of $T \sim 50 - 100$ K are located at radii of $r \approx 10 - 100$ AU (e.g., Kenyon, Calvet, & Hartmann 1993), consistent with the $0''.75$ (< 100 AU) source size of IRS3(A) (Fig. 1). Thus, the mid-infrared observations are probing directly the zone of accretion near, or at, the central protostar.

The detected mid-infrared radiation provides a means of estimating the central accretion luminosity. Summing over the dual blackbody curve from 5 – 30 μm , we estimate the mid-

infrared luminosity to be $L_{midir} = 1.3 \left(\frac{d}{300\text{pc}} \right)^2 L_{\odot}$. If all the mid-infrared luminosity is a result of gravitational infall, then we can estimate a central source mass from the relation $L = \frac{GM\dot{M}}{R_*}$, where \dot{M} is the mass infall rate, R_* is the source size, and M_* is the source mass. Using a standard $R_* = 3 R_{\odot}$ protostellar radius (Stahler, Shu, & Taam 1980) and typical mass accretion rates of $\dot{M} = 10^{-5} - 10^{-6} M_{\odot} \text{ yr}^{-1}$ (Kenyon, Calvet, & Hartmann 1993), we estimate the central mass to be $M_* = 0.02 - 0.2 M_{\odot}$.

3.2. Overall Spectral Energy Distribution

At $\lambda = 2.7$ mm, IRS3(A) and IRS3(B) have been spatially resolved as two distinct sources, but with a common envelope (Looney, Mundy, & Welch 2000). The 2.7 mm flux densities, integrated over $\sim 2.5''$ boxes, for IRS3(A) and IRS3(B) are $F_{2.7\text{mm}} = 0.019 \pm 0.004$ Jy and $F_{2.7\text{mm}} = 0.116 \pm 0.01$ Jy, respectively. At far-infrared wavelengths, the binary remains unresolved, with IRAS flux densities of $F_{60\mu\text{m}} = 29 \pm 6$ Jy and $F_{100\mu\text{m}} = 89 \pm 19$ Jy (Barsony et al. 1998). In Figure 3, we present the overall spectral energy distribution of IRS3(A).

The modified blackbody fit to the IRS3(A,B) common envelope (Barsony et al. 1998), scaled to the 2.7 mm flux of IRS3(A), is shown in Figure 3. The cold ($T = 22.5$ K) blackbody fit to the envelope clearly does not predict the observed mid-infrared luminosity. Unlike the prototypical class 0 sources (e.g., VLA 1623), the cold envelope emission does not dominate the overall SED of IRS3(A) (e.g., André, Ward-Thompson, & Barsony 2000).

Using spherical infalling envelope models (Terebey, Shu, & Cassen 1984; Kenyon, Calvet, & Hartmann 1993; Hartmann 1998), the envelope mass and bolometric luminosity of IRS3(A) can be estimated. The models (provided courtesy N. Calvet) have a density at $r = 1$ AU of $\rho_1 = 7.5 \times 10^{-14} \text{ g cm}^{-3}$, corresponding to an envelope infall rate of $\dot{M} \approx 10^{-5} M_{\odot} \text{ yr}^{-1}$. Models with centrifugal radii of $r_c = 50$ AU and 150 AU were tested. The centrifugal radius r_c represents the radius at which the spherical envelope departs from free-fall ($\rho \propto r^{-3/2}$) as material falls onto the disk ($\rho \propto r^{-1/2}$). The models have an inclination of $i \sim 60^\circ$ and a luminosity of $1 L_{\odot}$. A factor of 1.6 was needed to scale the models to the 2.7 mm flux, indicating that IRS3(A) is more luminous than $1 L_{\odot}$ (in agreement with the measured $L_{midir} = 1.3 L_{\odot}$). The model SEDs are shown in Figure 3.

The shape of the model SED and the depth of the silicate features are dependent upon the source luminosity, density, centrifugal radius, and source inclination. Detailed modeling of the SED cannot provide a unique solution without a much more complete SED for IRS3(A). However, representative models can qualitatively parameterize the luminosity

and the density of the protostar.

A model with $\rho_1 \approx 10^{-13}$ g cm $^{-3}$ and $\dot{M} \approx 10^{-5}$ M $_{\odot}$ yr $^{-1}$ provides a reasonable fit to the overall SED of IRS3(A) (see Figure 3). For this particular model density (ρ_1), the model with the smaller centrifugal radius (50 AU) best describes the data. If the density ρ_1 is decreased by an order of magnitude, then the models predict an infrared luminosity 10 – 100 times larger than that observed. If the density is increased by an order of magnitude, the models predict an infrared luminosity 10 – 100 times lower than that observed (e.g., Kenyon, Calvet, & Hartmann 1993; Hartmann 1998). These model densities and infall rates are more like those associated with the models for class I protostars such as L1551-IRS5 (e.g., Kenyon, Calvet, & Hartmann 1993; Hartmann 1998). Jayawardhana, Hartmann, & Calvet (2001) found that the true class 0 sources (VLA 1623 & HH24 MMS) require models with infall rates an order of magnitude higher than required for IRS3(A).

The bolometric luminosity of IRS3(A), estimated from the luminosity of the scaled infall model, is $L_{bol} \approx 1.6 L_{\odot}$, and the submm luminosity ($\lambda > 350$ μ m) is $L_{submm} \approx 10^{-4} L_{\odot}$. Thus, $L_{submm}/L_{bol} \sim 0.01\%$ is below the observational minimum for a class 0 protostar. The model envelope mass ($r > r_c$) is $M_{env} \approx 0.15 M_{\odot}$. Finally, the modeling suggests that the majority, if not all, of the far-infrared emission of IRS3(A,B) is also produced by IRS3(A).

3.3. Classification of IRS3

A key goal of the SED analyses is to clarify the evolutionary status of the IRS3 components. Class 0 to class I evolution is characterized by the transition from $M_{env} > M_*$ to $M_{env} < M_*$. The envelope mass for IRS3(A) was found to be $M_{env} \approx 0.15 M_{\odot}$, and depending upon the assumed infall rate \dot{M} , the IRS3(A) central source mass is estimated to be $M_* \sim 0.02 - 0.2 M_{\odot}$. Thus, the envelope and central star masses are comparable to each other.

Bontemps et al. (1996) established an empirical diagnostic $M_{env} - L_{bol}$ diagram that appears to naturally separate confirmed class 0 sources from confirmed class I sources (see also André, Ward-Thompson, & Barsony 2000). We have reproduced that diagram here (Figure 4) and have indicated the position of IRS3(A). The minimum L_{bol} is from the mid-infrared luminosity estimate ($1.3 L_{\odot}$) and the maximum is from the scaled infall model ($1.6 L_{\odot}$).

IRS3(A) falls squarely within the midst of the confirmed class I objects, and is fully separated from the class 0 protostars. The position of IRS3(A) in the $M_{env} - L_{bol}$ diagram, combined with the relative mass estimates from above, suggests that IRS3(A) may be more

evolved than a class 0 protostar. This may also explain why infall appears associated with IRS3(B) and not IRS3(A) (Terebey & Padgett 1997). The fact that IRS3(A) is invisible at near-infrared wavelengths may have more to do with the common envelope than the actual evolutionary status of IRS3(A). Perhaps IRS3(A) marks a transition between the class 0 protostar and the class I young stellar object.

We can also estimate the classification of IRS3(B) from the $M_{env} - L_{bol}$ diagram. The total luminosity of the binary is $L_{bol} = 10.9 L_{\odot}$ (Barsony et al. 1998). A range of $L_{bol} \approx 9.3 - 9.6 L_{\odot}$ can be assigned to IRS3(B), if we associate $1.3 - 1.6 L_{\odot}$ to IRS3(A). The envelope mass, as determined from the 2.7 mm flux density, is $M_{env} \approx 0.5 M_{\odot}$. On the $M_{env} - L_{bol}$ diagram, these values place IRS3(B) among the class 0 sources. If IRS3(A) and IRS3(B) are indeed coeval, then the apparent classification difference between the two sources may yield information about how binary stars evolve and how they interact with each other and/or their environments.

4. Summary

We have obtained high angular resolution ($\sim 0''.5$) $10 - 25 \mu\text{m}$ imaging of the protostellar binary system L1448N-IRS3(A,B). These observations mark the first time the sources have been spatially resolved at wavelengths $\lambda < 2.7 \text{ mm}$. The binary, as a whole, had been previously classified as a class 0 protostar. The primary result of the work is that only one source, IRS3(A), was detected at mid-infrared wavelengths. That is, all of the mid-infrared emission from IRS3(A,B) emanates from IRS3(A). The mid-infrared luminosity of IRS3(A) is $L_{midir} = 1.3 L_{\odot}$. The central source mass ($0.02 - 0.2 M_{\odot}$) of IRS3(A) is comparable to its envelope mass ($0.15 M_{\odot}$).

IRS3(A), with a $L_{submm}/L_{bol} \sim 0.01\%$ and an infall rate of $10^{-5} M_{\odot} \text{ yr}^{-1}$, may be more akin to the class I protostars. The common envelope surrounding IRS3(A) and IRS3(B) may skew the appearance of IRS3(A). Perhaps IRS3(A) is viewed at a particular angle that gives it the appearance of both a class 0 and class I source, or perhaps IRS3(A) is a transition object between the two classes. IRS3(B), invisible at near and mid-infrared wavelengths, appears to possess a SED dominated by the cold envelope, indicating that IRS3(B) may be a true class 0 protostar. Spatially resolved far-infrared observations ($\lambda = 30 - 300 \mu\text{m}$) with SIRTf, coupled with detailed modeling, are needed to determine the relative contributions of IRS3(A) and IRS3(B) to the emission near the peak of the spectral energy distributions, and the relative evolutionary status of the two sources.

The authors would like thank the Gemini staff for their help and outstanding support

in making OSCIR a success on Gemini-North. The UF team would especially like to thank Chris Carter, who endured some long nights at the telescope while the astronomers worked - although the wee dram or two at the end was probably worth it. D.R.C. would like to thank N. Calvet for her kind and helpful discussions and for providing the protostar models in numerical format. The authors would like to thank the referee, whose comments led to a better paper. J.P.W. acknowledges support by NSF grant AST-0134739. C.M.T. acknowledges support by NSF grant AST-0098392.

Based on observations obtained at the Gemini Observatory, which is operated by the Association of Universities for Research in Astronomy, Inc., under a cooperative agreement with the NSF on behalf of the Gemini partnership: the National Science Foundation (United States), the Particle Physics and Astronomy Research Council (United Kingdom), the National Research Council (Canada), CONICYT (Chile), the Australian Research Council (Australia), CNPq (Brazil) and CONICET (Argentina). This paper is based on observations obtained with the mid-infrared camera OSCIR, developed by the University of Florida with support from the National Aeronautics and Space Administration, and operated jointly by Gemini and the University of Florida Infrared Astrophysics Group.

REFERENCES

- Adams, F. C., Lada, C. J., & Shu, F. H. 1987, *ApJ*, 312, 788
- André, P. & Montmerle, Th. 1994, *ApJ*, 420, 837
- André, P., Ward-Thompson, D., & Barsony, M. 2000, in Mannings V., Boss A. P., Russell S. S., eds, *Protostars and Planets IV*. Univ. Arizona Press, Tucson, p. 59
- André, P., Ward-Thompson, D., & Barsony, M. 1993, *A&A*, *ApJ*, 420, 837
- Bachiller, R., Cernicharo, J., Martin-Pintado, J., Tafalla, M., & Lazereff, B. 1990, *A&A*, 231, 174
- Barsony, M., & Kenyon, S. J. 1992, *ApJ*, 384, L53
- Barsony, M., Ward-Thompson, D., André, P., & O’Linger, J 1998, *ApJ*, 509, 733
- Bontemps, S., André, P., Terebey, S., & Cabrit, S. 1996, *A&A*, 311, 858
- Chen, H., Grenfell, T. G., Myers, P. C., & Hughes, J. D. 1997, *ApJ*, 478, 295
- Chen, H., Myers, P. C., Ladd, E. F., & Wood, D. O. S. 1995, *ApJ*, 445, 377

- Curiel, S., Raymond, J. C., Rodríguez, R., Cantó, J., & Moran, J. M. 1990, *A&A*, 365, L85
- Davis, C. J., Dent, W. R. F., Matthews, H. E., Aspin, C., & Lightfoot, J. F. 1994, *MNRAS*, 266, 933
- Davis, C. J. & Smith, M. D. 1995, *ApJ*, 443, L41
- Guilloteau, S., Bachiller, R., Fuente, A., & Lucas, R. 1992, *A&A*, 265, L49
- Hartmann, L. 1998, *Accretion Processes in Star Formation*, Cambridge University Press, New York
- Jayawardhana, R., Hartmann, L. & Calvet, N. 2001, *ApJ*, 548, 310
- Kenyon, S. J., Calvet, N., & Hartmann, L. 1993, *ApJ*, 414, 676
- Lada, C. J. 1987, in *IAU Symp. 115 Star Forming Regions*, ed. M. Peimbert & J. Jugaku (Dordrecht: Reidel), 1
- Lada, C. J. & Wilking, B. A. 1984, *ApJ*, 287, 610
- Looney, L. W., Mundy, L. G., & Welch, W. J. 2000, *ApJ*, 529, 477
- Masunaga, H. & Inutsuka, S. 2000, *ApJ*, 531, 350
- Saraceno, P., André P., Ceccarelli, C., Griffin, M., & Molinari, S. 1996, *A&A*, 309, 827
- Shirley, Y. L., Evans, N. J. II, Rawlings, J. M. C., & Gregersen, E. M. 2000, *ApJS*, 131, 249
- Stahler, S., Shu, F. H., & Taam, R. E. 1980, *ApJ*, 242, 226
- Terebey, S., Chandler, C. J., & André, P. 1993, *ApJ*, 414, 759
- Terebey, S., Shu, F. H., & Cassen, P. 1984, *ApJ*, 286, 529
- Tereby, S., & Padgett, D. 1997, in *IAU Symp. 182, Herbig-Haro Flows and the Birth of Low-Mass Stars*, ed. B. Reipurth & C. Bertout (Dordrecht: Kluwer)

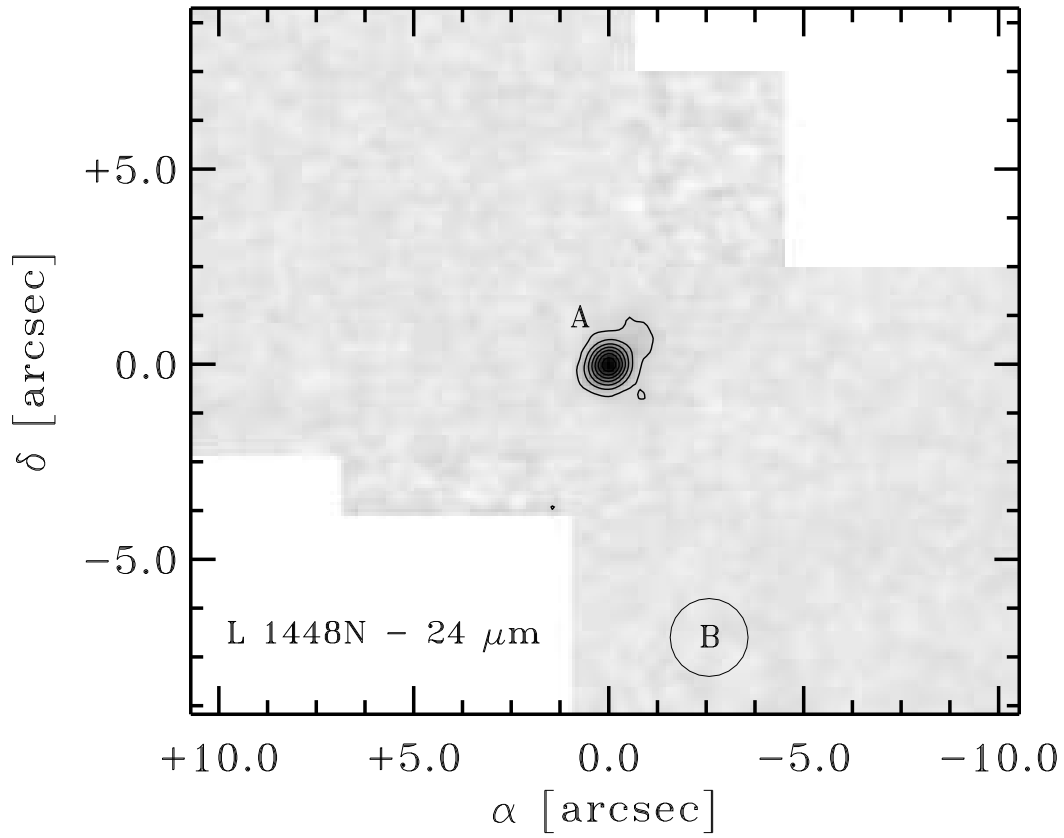


Fig. 1.— 24 μm image of L 1448N-IRS3, smoothed with an $0''.4$ gaussian. Only IRS3(A) is detected. The position of IRS3(B) is marked by the open circle. The contours start at 0.6 Jy/arcsec^2 and are stepped by 1.0 Jy/arcsec^2 . $(0, 0) = \alpha(J2000) = 03^{\text{h}} 25^{\text{m}} 36.5^{\text{s}}$, $\delta(J2000) = 30^{\circ} 45' 21''$.

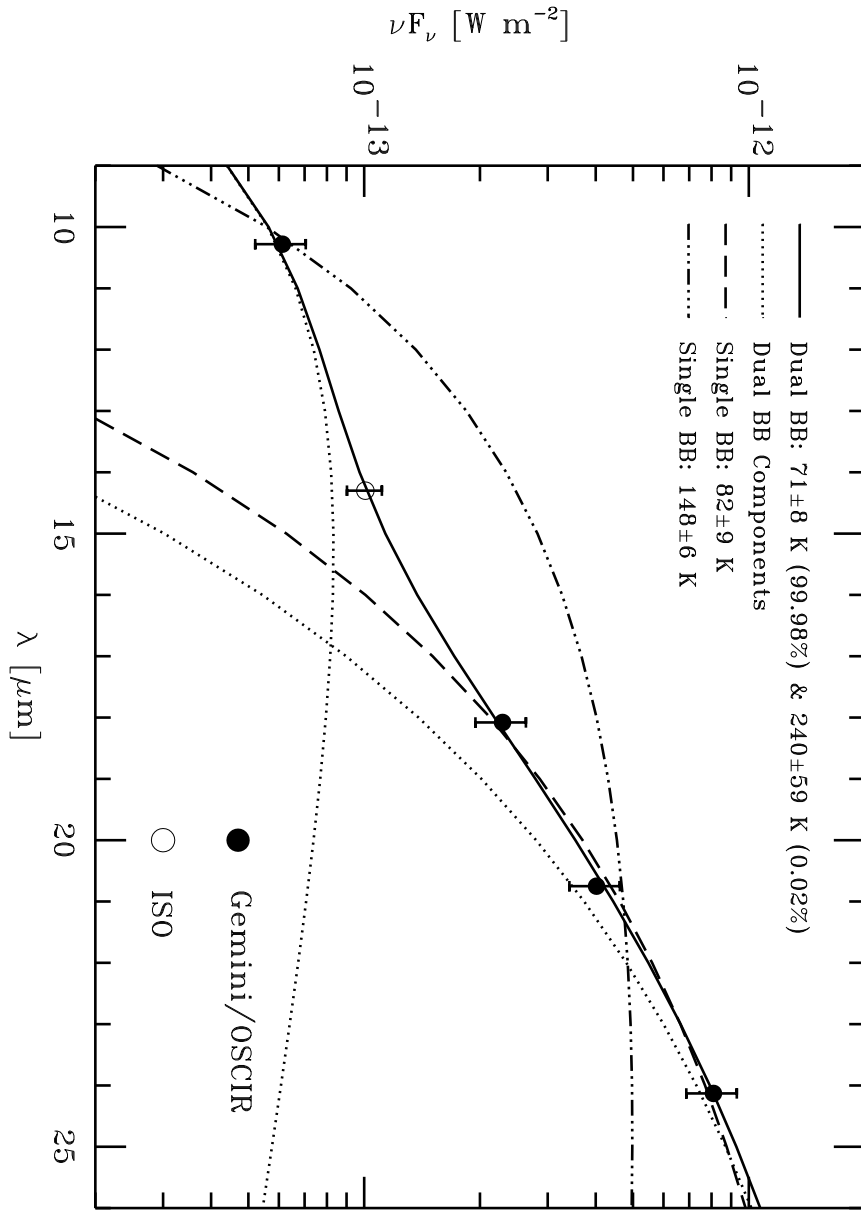


Fig. 2.— Mid-infrared spectral energy distribution for IRS3(A). The 148 K single blackbody curve was fitted to all of the mid-infrared data, and the 82 K single blackbody curve was fitted to only the OSCIR IHW18, Q3, & H25 filter points. The dual blackbody curve was fitted to all of the mid-infrared data; the individual components of the dual blackbody are also shown.

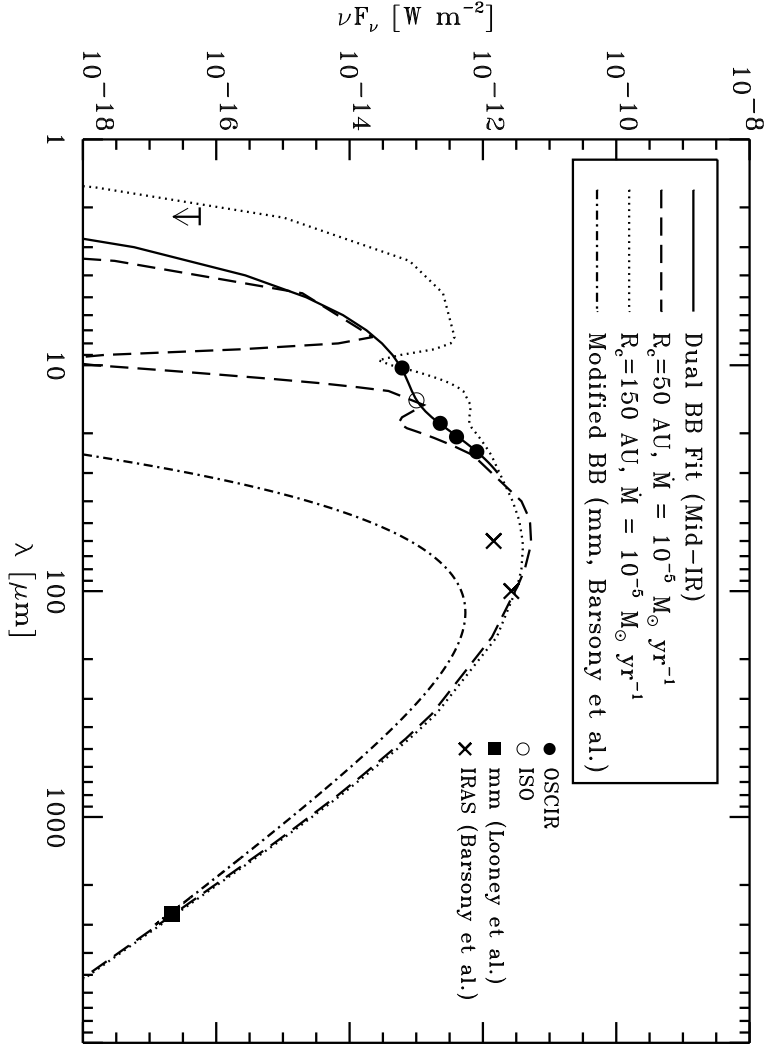


Fig. 3.— Spectral energy distribution for IRS3(A), including the $K > 18$ mag upper limit (Terebey & Padgett 1997). The 60 & 100 μm IRAS data represent the total (unresolved) far-infrared flux of the binary. The dual blackbody curve is from Figure 2, and the modified blackbody function, scaled to the $\lambda = 2.7$ mm flux, is from Barsony et al. (1998). The dashed and dotted curves represent spherical infalling envelope models (courtesy N. Calvet).

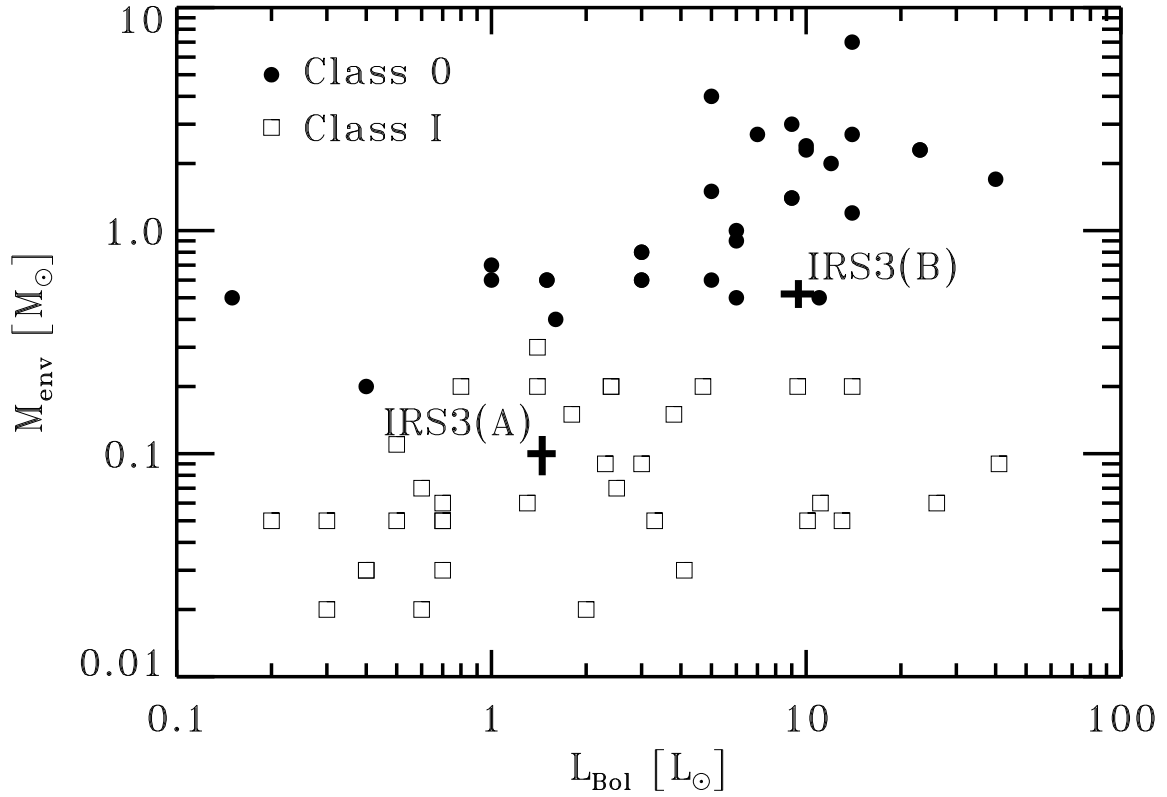


Fig. 4.— Envelope mass versus bolometric luminosity is plotted for a set of Class 0 and Class I protostars. Figure and data adapted from Bontemps et al. (1996) and André, Ward-Thompson, & Barsony (2000). The positions of IRS3(A) & IRS3(B) are also shown.

Table 1. Summary of Observations

Filter	λ_c (μm)	$\Delta\lambda$ (μm)	Frametime (ms)	On-Source (min)	Airmass
N	10.38	5.23	7	2	1.5
IHW18	18.08	1.65	13	2	1.4
Q3	20.75	1.65	13	2	1.3
H25	24.13	3.6	7	6 ^a	1.2 – 1.3

^aSummation of 3-position mosaic with 2 minutes per position.

Table 2. IRS3 Mid-Infrared Photometry

Filter	IRS3(A) F_ν (Jy)	IRS3(B) ^a F_ν (Jy)
N	0.21 ± 0.01	< 0.03
IHW18	1.38 ± 0.02	< 0.06
Q3	2.78 ± 0.04	< 0.12
H25	6.51 ± 0.08	< 0.24

^a 3σ upper limits.